

# Influence of Isothermal Heating on the Curie Temperature of FeCoB Bulk Amorphous Alloy

KINGA JEZ, BARTLOMIEJ JEZ\*, PAWEŁ PIETRUSIEWICZ

Institute of Physics, Faculty of Production Engineering and Materials Technology, Czestochowa University of Technology, 19 Armii Krajowej Str., 42-200 Czestochowa, Poland

*The article presents the results of research on the thermal treatment of amorphous alloys. As part of the work, an alloy with a chemical composition  $Fe_{63}Co_8Y_8W_1B_{20}$  was produced by rapid cooling. The method used to aspirate the liquid alloy into the copper mold was used. The produced material was subjected to annealing at 940K for 10 minutes. The alloy, after solidification and after heat treatment, was subjected to structure testing by means of X-ray diffraction. The soaking process led to the partial crystallization of the amorphous precursor. Using the Faraday magnetic balance, curves of the magnetic saturation polarization as a function of temperature were recorded, on the basis of their analysis, the Curie temperature of the produced materials was determined. Using the vibration magnetometer, the primary curves of magnetization and static magnetic hysteresis loops were measured. The alloy after the soaking process was characterized by higher Curie temperature and magnetically hard properties. The test results confirm the possibility of modifying the magnetic properties of high-temperature alloys through a suitably designed heat treatment.*

*Keywords: bulk amorphous materials, nanocrystalline materials, Curie temperature, isothermal heating, vibration magnetometer*

Rapid-cooled alloys due to their properties belong to the so-called functional materials. These materials include, among others, amorphous and nanocrystalline alloys. Amorphous alloys have been known for several decades, initially they were produced in the form of thin strips and layers [1]. Amorphous materials exhibit a disordered structure similar to liquids. However, the liquid structure preserved for the solidified material generates completely new properties, often much better than their crystalline counterparts [2]. Amorphous materials exhibit so-called soft magnetic properties, including a low coercive field value and high saturation magnetisation [3-15].

One of the ways of obtaining amorphous materials is the rapid cooling of liquid alloys. During this process the glass structure suitable for liquids is vitrified. A well-known method of producing amorphous materials is cooling the liquid alloy on a copper cylinder. This method is characterized by a cooling rate of  $10^6$  K/s [16]. Such a high cooling rate prevents the production of volatile amorphous alloys. Produced tapes and layers with a thickness of 50  $\mu$ m significantly reduce the applicability of these materials. Therefore, over the years, scientists sought a way to produce materials with an amorphous structure with a much lower cooling rate. The breakthrough was the study of A. Inoue, who put forward three empirical principles according to which amorphous materials should be produced. Negative heat of mixing, multi-components of the alloy and correspondingly large differences in the length of atomic rays of the main alloy components significantly increase the chance of producing alloys with amorphous structure [17]. The use of these principles affects the melt viscosity. The mutual blocking of atoms in the volume of the alloy during its cooling prevents them from diffusing into larger distances, which stops the process of crystallization and maintains the chaotic arrangement of atoms in the volume of the sample. The new group of alloys is called bulk amorphous materials [18-22].

Controlled crystallization of amorphous precursors can give these materials completely new properties. Two-phase materials consisting of an amorphous matrix and a

crystallite size not exceeding 100 nm in its volume often have better magnetic properties as compared to amorphous precursors [23]. So-called nanocrystalline materials can be produced by suitably selected heat treatment of the amorphous alloy. By means of isothermal annealing it is possible to influence their magnetic properties such as saturation magnetization, coercive field value or Curie temperature. Proper selection of the chemical composition enables the production of a nanocrystalline alloy in a one-step process during the rapid cooling of the liquid alloy.

The aim of the work is to produce a bulk rapid-cooled alloy with chemical composition  $Fe_{63}Co_8Y_8W_1B_{20}$  by aspirating a liquid alloy into a copper mold and determining the influence of annealing on the Curie temperature of the tested alloy. The research methods used to determine the structure (X-ray diffraction) and selected properties of manufactured materials (Faraday magnetic balance) were used in the work.

## Experimental part

### Studied material

The batch material for making the high temperature melt was prepared using an arc furnace. The elements used to produce polycrystalline ingots were characterized by purity above 99.99%. Five gram samples were weighed out. The remelting of the material was carried out in a protective atmosphere of argon after earlier generation of a high vacuum in the working chamber of the arc furnace. In addition, the working chamber was flushed with argon. These treatments are aimed at getting the most neutral atmosphere. In particular, it is important to eliminate oxygen from the working chamber, which causes the formation of heterogeneous seeds of crystallization, which is an undesirable phenomenon hindering the formation of amorphous structure of cast alloys. The polycrystalline ingots were smelted with a plasma arc, the temperature of which is regulated by the intensity of current flowing through the electrode. Before the actual melting process, the ingot was melted with pure titanium. Due to its

\* email: bartek199.91@o2.pl

properties, the melted titanium absorbs the remaining impurities in the working chamber, which further improves the purity of the atmosphere prevailing in the working chamber. The ingot was melted 7 times by turning it over to the other side using the manipulator before each subsequent melting. Purified and crushed into smaller pieces of ingots, it was used to produce a rapid-cooled alloy.

The polycrystalline ingot is placed in a hollow water-cooled copper plate. The disc also has space for pure titanium. The remelting of pure titanium before the process of casting a molten alloy into the copper mold greatly improves the possibility of creating in its volume the amorphous structure. The process for producing the high-temperature melt is carried out under similar conditions as in the production of polycrystalline ingot. A high vacuum was created in the working chamber, after which it was rinsed with argon and pumped down again. The process of pouring the molten alloy into the copper mold was carried out at an argon pressure of 0.7 bar. Melted using a plasma arc, the alloy is sucked into the copper mold by means of a pump system and valves. The alloy was obtained in the form of 0.5 mm thick plates. The produced material was heat treated. The alloy sample was heated at 940K for 10 minutes. The heating of the amorphous alloy at a temperature close to the crystallization temperature should result in nanocrystallization of the structure. The alloy was subjected to structure testing after solidification and after heat treatment. The X-ray diffractometer from BRUCKER model Advanced 8 was used. The X-ray diffraction was carried out in the 2 theta angle range from 30° to 100° with a 0.02° measuring step and an exposure time of 6 seconds.

The phase analysis of the obtained material after heat treatment was carried out using the specialist Match! Program. The sizes of the identified crystal phase grains were estimated using the Scherrer formula:

$$D = (\lambda * K) / 2 \beta_{\theta} \cos\theta \quad (1)$$

where:

- K -Scherrer shape coefficient (K = 0.91),
- $\lambda$  -characteristic wavelength,
- $\beta_{\theta}$  -half width in the middle of the peak intensity (background is included),
- $\theta$  -Bragg angle.

Using the Faraday magnetic balance, magnetic saturation polarization curves were recorded as a function of temperature for the alloy samples in the state after solidification and after heating. The measurement was carried out in the temperature range from room temperature to 850K. The curves were recorded in the direction of rising temperatures and in the reverse direction during cooling of the samples.

Using the vibration magnetometer, static magnetic hysteresis loops were measured. The measurement was carried out at the induction of an external magnetic field from 0 to 2 T.

## Results and discussions

Figure 1 shows the X-ray diffraction pattern for the  $\text{Fe}_{63}\text{Co}_8\text{Y}_8\text{W}_1\text{B}_{20}$  alloy in the state after solidification.

The registered diffractogram pattern is typical for amorphous materials. In the examined range of the angle 2 theta from 30° to 100° only the broad maximum called the amorphous hall is visible. There are no peaks indicating the presence of grains of crystalline phases in the volume of the sample.

Figure 2 shows the X-ray diffraction pattern of the  $\text{Fe}_{63}\text{Co}_8\text{Y}_8\text{W}_1\text{B}_{20}$  alloy after heating.

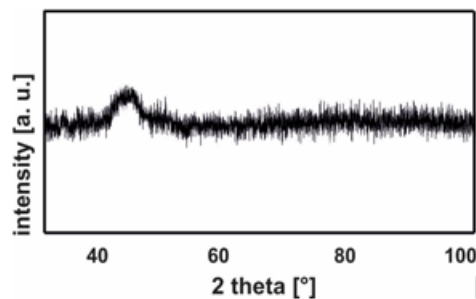


Fig. 1. X-ray diffractogram for the  $\text{Fe}_{63}\text{Co}_8\text{Y}_8\text{W}_1\text{B}_{20}$  alloy sample in as-solidified state

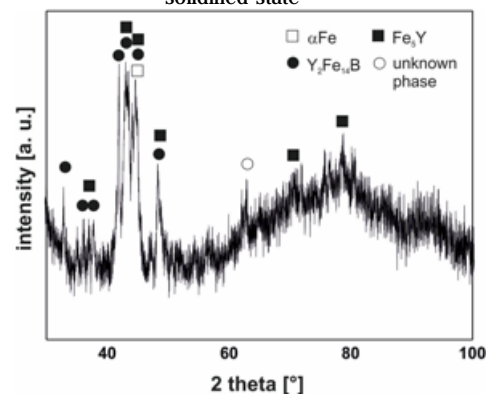


Fig. 2. X-ray diffractogram for the  $\text{Fe}_{63}\text{Co}_8\text{Y}_8\text{W}_1\text{B}_{20}$  alloy sample after annealing 940K/10min

Annealing of the alloy sample  $\text{Fe}_{63}\text{Co}_8\text{Y}_8\text{W}_1\text{B}_{20}$  at 940K for 10 minutes, it resulted in partial crystallization of the alloy. The registered diffractogram indicates obtaining a two-phase material. On the diffractogram, a wide maximum in the range of 40 theta angle 40°-50° from the amorphous phase is visible. Visible are narrow peaks derived from the grains of crystalline phases. Table 1 presents the estimated sizes of the resulting crystal grains. The determined sizes of the resulting crystallites do not exceed 100 nm, which classifies the produced material as nanocrystalline [24].

**Table 1**

DATA OBTAINED FROM THE X-RAY DIFFRACTOGRAM ANALYSIS (FIG. 2) USING THE SCHERRER FORMULA FOR SAMPLES AFTER ANNEALING (940K/10 MIN)

alloy/phase	$\alpha$ - Fe [nm]	$\text{Fe}_3\text{Y}$ [nm]	$\text{Fe}_{14}\text{Y}_2\text{B}$ [nm]
$\text{Fe}_{63}\text{Co}_8\text{Y}_8\text{W}_1\text{B}_{20}$	15.6	16.8	24.8

In the volume of the alloy, the iron-rich magnetic phases were identified: the soft magnetic phase  $\alpha\text{Fe}$ , the magnetic phase, the semi-hard  $\text{Fe}_3\text{Y}$ , and the magnetically hard  $\text{Fe}_{14}\text{Y}_2\text{B}$  phase. Figure 3 shows the curves of magnetic polarization as a function of temperature for the prepared alloy samples  $\text{Fe}_{63}\text{Co}_8\text{Y}_8\text{W}_1\text{B}_{20}$ .

Magnetic polarization decreases with increasing temperature. On the curve (fig. 3a) there is only a clear deflection below the temperature of 600K indicating that the material has passed from the ferromagnetic to the paramagnetic state. In the case of a sample of the alloy after annealing, on the thermomagnetic curve, two inflections are visible which indicates the presence of at least two ferromagnetic phases in the volume of the tested sample. The first inflection in this case comes from the crystalline phase  $\text{Fe}_{14}\text{Y}_2\text{B}$ , which is confirmed by the analysis of X-ray diffraction images. The second phase is an amorphous matrix. Magnetization at 850K still does not reach 0, which means the presence of a certain number of other magnetic phases in the volume of the alloy sample. These phases up to a temperature of 850K are characterized by ferromagnetic properties. The magnetic saturation polarization curves measured in the

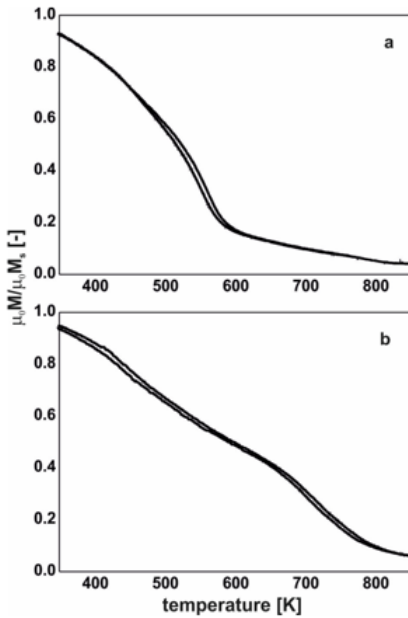


Fig. 3. Magnetic saturation polarization as a function of temperature for alloy  $Fe_{63}Co_8Y_8W_1B_{20}$ : a) as-solidified state, b) after annealing 940K/10min

direction of decreasing temperatures almost coincide with the curves measured in the direction of sample heating. This proves the good thermomagnetic stability of the materials produced. Small differences in the course of recorded curves are derived from the partial relaxation of the amorphous structure, which occurs during the measurement. Figure 4 shows the curves  $\mu_0 M_s^{(1/b)}$  as a function of temperature.

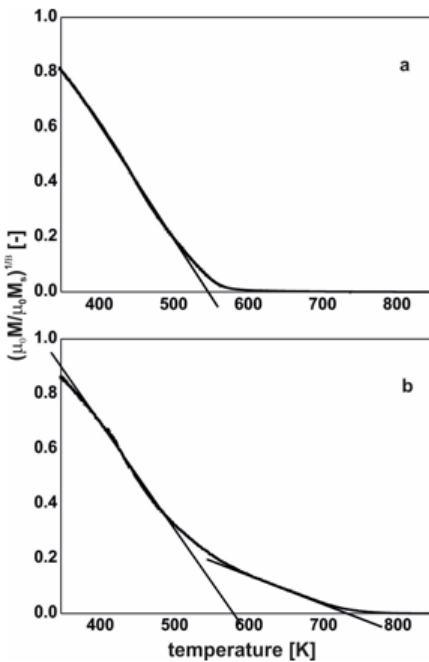


Fig. 4. Curves  $\mu_0 M_s^{(1/b)}$  as function of temperature for  $Fe_{63}Co_8Y_8W_1B_{20}$  alloy: a) as-solidified state, b) after annealing 940K/10min

For ferromagnetics that meet the Heisenberg assumptions, it is possible to determine the Curie temperature using a critical coefficient of  $\beta = 0.36$ . For the alloy in the solidified state, a Curie temperature of 550K. was determined. In the case of an alloy, after the heating, two Curie temperatures were determined. On the basis of the X-ray diffractogram analysis (Fig. 2), it was found that the first Curie temperature of 595K comes from the  $Fe_{14}Y_2B$  phase transition from ferro to paramagnetic. The second designated Curie temperature is 710K. It should be assumed that this is the temperature corresponding to the transition from the ferro to paramagnetic amorphous matrix, which remained in the melt volume after the heating process. The other Curie temperature value than the alloy in the solidified state indicates a change in the chemical composition of the amorphous phase present in the

melt sample subjected to annealing. The iron-rich crystalline phases explain this phenomenon. The phases absorbing iron, boron and yttrium from the volume of the amorphous phase cause an increase in the concentration of cobalt in the amorphous matrix. It is known that a small addition of cobalt significantly increases the Curie temperature [25]. The measuring range up to 850K does not allow registering the inflection associated with the transition from ferro to paramagnetism for the remaining phases occurring in the sample volume ( $Fe_2Y$ ,  $\alpha Fe$ ). The Curie temperature of these phases is much higher than 850K.

Figure 5 presents the primary magnetization curves for samples of the tested alloy.

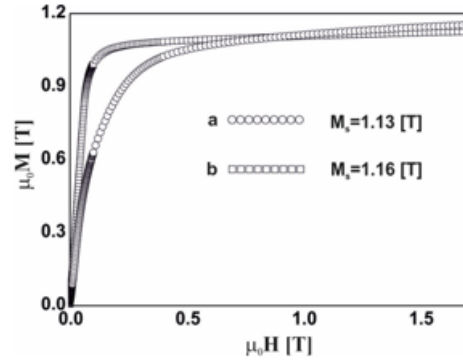


Fig. 5. Primary magnetization curves for alloy: a) as-solidified state, b) after annealing 940K/10min

The primary magnetization curves indicate an easier course of the magnetization of the sample in the solidified state. The magnetization of this sample reaches a high value at a much lower external magnetic field.

Figure 6 presents static magnetic hysteresis loops measured for the produced alloy samples  $Fe_{63}Co_8Y_8W_1B_{20}$ . The static magnetic hysteresis loop for the alloy sample in the solidified state is typical as for magnetic materials exhibiting magnetically soft properties. The loop measured for the alloy sample after heating at 940 K for 10 minutes has an osmotic shape, which indicates the presence of a hard magnetic or semi-hard phase in the volume of the

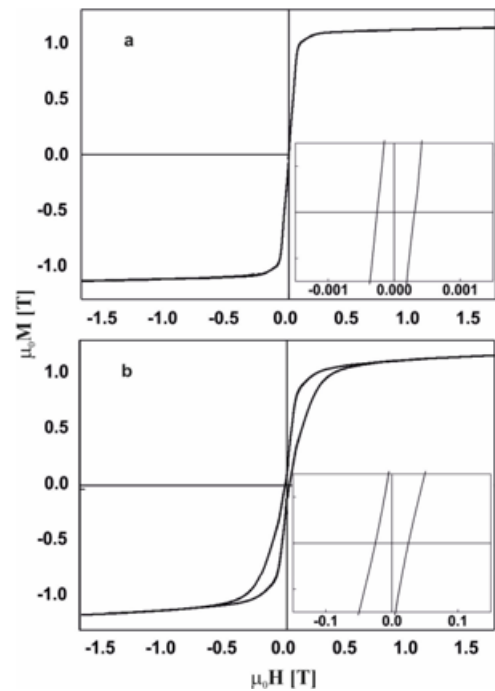


Fig. 6. Static magnetic hysteresis loops measured for the alloy  $Fe_{63}Co_8Y_8W_1B_{20}$ : a) as-solidified state, b) after annealing 940K/10min

sample [26]. The alloy in the state after solidification possesses magnetization of saturation at the level of 1.13 T and value of coercive field 223 A/m, which allows to classify the tested alloy as a material with magnetically soft properties. Annealing of the alloy caused the saturation magnetization to increase to 1.16 T and the coercive field value to 19820 A/m, which qualifies the material as magnetically hard. The increase in saturation magnetization can be associated with the formation of a soft magnetic phase  $\alpha$ Fe.

The results obtained during the vibration magnetometer measurements confirm and supplement the analysis of thermomagnetic curves (figs. 3 and 4) and X-ray diffraction patterns (Fig. 1 and 2). The phase  $\text{Fe}_{14}\text{Y}_2\text{BFe}_3\text{Y}$  corresponds to an almost 100-fold increase in the coercive field value. These phases were identified based on the X-ray diffractogram, and the Curie temperature was also determined for  $\text{Fe}_{14}\text{Y}_2\text{B}$  phase.

Figure 7 presents the analysis of the primary magnetization curve in the area called the approach to ferromagnetic saturation. The analysis showed that the process of magnetizing the sample in the field of magnetic field induction 0.064 - 0.33 T is related to the rotation of the magnetization vector around linear defects of the structure in the form of pseudo-location dipoles, for which the relationship is satisfied:

$$\frac{a_2}{\mu_0 H^2} = 0,456 \mu_0 \frac{G^2 \lambda_s^2}{(1-\nu)^2} \frac{N b_{df}}{M_s^2} D_{df}^2 \frac{1}{(\mu_0 H)^2} \quad (2)$$

where:  $M_s$  -spontaneous magnetization,  $H$  - magnetic field,  $a_2$  -Angular coefficient of linear fit, corresponding to linear defects,  $D_{df}$  -width of the pseudo-dislocation dipole,  $\mu_0$  -magnetic vacuum permeability,  $G$  -transverse elastic shear module,  $\nu$  - Poisson coefficient,  $\lambda_s$  -magnetostriction constant.

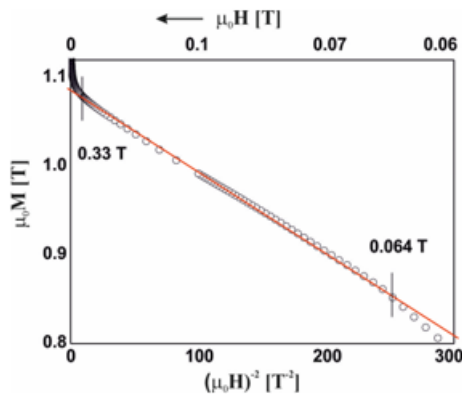


Fig. 7. Dependence of  $\mu_0 M ((\mu_0 H)^{-2})$  for  $\text{Fe}_{63}\text{Co}_8\text{Y}_8\text{W}_1\text{B}_{20}$  alloy as-solidified state

In the case under study, the sizes of the line defects are greater than the exchange distance:  $D_{df} > l_H$ . Figure 8 presents the magnetization curves as a function  $(\mu_0 H)^{1/2}$ .

Above the area of the approach to ferromagnetic saturation, the process of magnetizing the material is associated with the suppression of thermally excited spin waves.  $D_{sp}$  is related to the parameter  $b$ , which can be described by the relationship [27]:

$$b = 3,54 g \mu_0 \mu_B \left( \frac{1}{4\pi D_{sp}} \right)^{3/2} kT (g \mu_B)^{1/2} \quad (3)$$

where:  $k$  -Boltzman's constant,  $\mu_B$  -Bohr magneton,  $g$  -gyromagnetic factor.

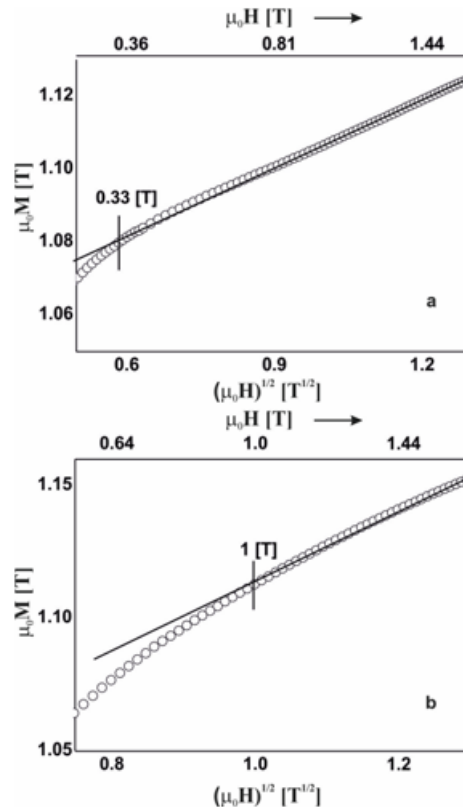


Fig. 8. High-field magnetic polarization curves as a function of  $(\mu_0 H)^{1/2}$  for  $\text{Fe}_{63}\text{Co}_8\text{Y}_8\text{W}_1\text{B}_{20}$  alloy: a) as-solidified state, b) after annealing 940K/10min

Based on the dependence (3), the spin wave stiffness parameter was calculated  $D_{sp}$ . The  $D_{sp}$  parameter for the alloy in the solidified state is  $42 \text{ meVnm}^2$ . The value of this coefficient for the alloy sample subjected to annealing at 940K in 10 min is  $26 \text{ meVnm}^2$ . The smaller value of the  $D_{sp}$  parameter is related to the change in the distance between  $\text{sp}^2$  magnetic atoms Co-Co, Fe-Co and Fe-Fe.

## Conclusions

The purpose of the work was to produce an amorphous alloy with a chemical composition  $\text{Fe}_{63}\text{Co}_8\text{Y}_8\text{W}_1\text{B}_{20}$  and to conduct a study of the structure and properties of the obtained material in the state after solidification and after heating. The method of aspirating the liquid alloy into the copper mold allows obtaining a volumetric basis based on iron with an amorphous structure. Designed thermal treatment allowed to obtain a material with a nanocrystalline structure consisting of an amorphous matrix and the crystal phases  $\alpha$  Fe,  $\text{Fe}_3\text{Y}$  and  $\text{Fe}_{14}\text{Y}_2\text{B}$  distributed in its volume of grains. The estimated values in the sample volume of crystallites do not exceed 100 nm. It turns out that heating an amorphous precursor at a temperature just below its crystallization temperature allows to influence the Curie temperature change of the material produced. Annealing has a significant effect on the magnetic properties of the alloy. The crystalline phases generated during this process influenced the increase in the saturation magnetization and the coercive field. The value of parameter  $D_{sp}$  is lower for the sample subjected to annealing. In this case, the value of this coefficient does not correlate with the increase in the saturation of the sample. This is related to the fact that crystalline phases are responsible for increasing the magnetization of the sample. In the case of an amorphous matrix, the higher value of the parameter  $D_{sp}$  is related to the distances between the magnetic atoms Co-Co, Fe-Co and Fe-Fe.

## References

1. KLEMENT, W., WILLENS, R.H., DUWEZ P., *Nature*, **187**, 1960, p. 869-870.
2. INOUE, A., YANO, N., MASUMOTO, T., *J. Mater. Science*, **19**, 1984, p. 3786-3795.
3. HAN, Y., CHANG, C.T., ZHU, S.L., INOUE, A., LOUZGUINE-LUZGIN, D.V., SHALAN, E., AL-MARZOUKI, F., *Intermetallics*, **54**, 2014, p. 169-175
4. HERZER, G., *Acta Materialia*, **61**, 2013, p. 718-734
5. CHIRIAC, H., LUPU, N., *Physica B: CONDENSED MATTER*, **299**, 2001, p. 293-301.
6. NABIALEK, M, JEZ, B, JEZ, K., *Rev. Chim. (Bucharest)*, **69**, no. 9, 2018, p. 2546-2550
7. NABIALEK, M., JEZ, B., BŁOCH, K., PIETRUSIEWICZ, P., GONDRO, J., *Journal of Magnetism and Magnetic Materials*, **477**, 2019, p. 214-219.
8. SI, J., DU, C., WANG, T., WU, Y., WANG, R., HUI, X., *Journal of Alloys and Compounds*, **741**, 2018, p. 542-548.
9. WANG, F., INOUE, A., HAN, Y., KONG, F.L., ZHU, S.L. SHALAN, E., AL-MARZOUKI, F., OBAID, A., *Journal of Alloys and Compounds*, **711**, 2017, p. 132-142.
10. LI, W., YANG, Y.Z., XU, J., *Journal of Non-Crystalline Solids*, **461**, 2017, p. 93-97.
11. BERE, P., DUDESCU, M.C., BALC, N., BERCE, P., IURIAN, A.M., NEMES, O., *Mat. Plast.*, **51**, no. 2, 2014, p. 145.
12. MINCIUNA, M.G., ACHITEI, D.C., VIZUREANU, P., SANDU, A.V., NABIALEK, M., *Acta Physica Polonica A*, **135**, no. 2, 2019, p. 115.
13. BORDEI, M., SANDU, A.V., PAPADATU, C.P., SANDU, I.G., *Rev. Chim. (Bucharest)*, **69**, no. 3, 2018, p. 632.
14. PAPADATU, C.P., SANDU, I.G., BORDEI, M., NABIALEK, M., SANDU, A.V., *Mat. Plast.*, **53**, no. 4, 2016, p. 771.
15. PAPADATU, C.P., SANDU, A.V., BORDEI, M., SANDU, I.G., *Rev. Chim. (Bucharest)*, **67**, no. 11, 2016, p. 2306
16. CHEN, H. S., MILLER, C. E., *Review of Scientific Instruments*, **41**, 1970, p. 1237.
17. INOUE, A., KATO, A., ZHANG, T., KIM, S.G., MASUMOTO, T., *Materials Transaction JIM*, **32**, 1991, p. 609-616.
18. NABIALEK, M., *Arch. Metall. Mater.*, **61**, 2016, p. 439-444.
19. INOUE, A., SHEN, B., OHSUNA, T., *Mater. Trans.*, **43**, 2002, p. 2337-2341.
20. LI, J.F., LIU, X., ZHAO, S.F., DING, H.Y., YAO, K.F., *J. Magn. Magn. Mater.*, **386**, 2615, p. 107-110.
21. REZAEI-SHAHREZA, P., SEIFODDINI, A., HASANI, S., *Journal of Non-Crystalline Solids*, **471**, 2017, p. 286-294.
22. SI, J., MEI, J., WANG, R., CHEN, X., HUI, X., *Materials Letters*, **181**, 2016, p. 282-284.
23. GONDRO, J., *J. Magn. Magn. Mater.*, **432**, 2017, p. 501-506.
24. LEONOWICZ, M., *Nanokrystaliczne materiały magnetyczne*, WNT, Warszawa 1998.
25. JEZ, B., *Rev. Chim. (Bucharest)*, **68**, no. 8, 2017, p. 1903-1907.
26. BŁOCH, K., NABIALEK, M., GARUS, S., *Acta Physica Polonica A*, **130**, 2016, p. 905-908.
27. KOHMOTO, O., *Journal Applied Physics*, **53**(11), 1982, p. 7486-7490.

---

Manuscript received: 9.07.2019